Materials and Structures, 1992, **25**, 327–334

Measurement of the fracture energy using three-point bend tests: Part 3 – Influence of cutting the P–δ tail

M. ELICES, G. V. GUINEA, J. PLANAS

Departamento de Ciencia de Materiales, Escuela de Ingenieros de Caminos, Universidad Politécnica, Ciudad Universitaria, 28040 Madrid, Spain

Available measures of the fracture energy G_F obtained with the procedure proposed by RILEM TC-50 provide values that appear to change with sample size, calling into question the possibility of considering G_F as a material parameter. In previous papers several sources of energy dissipation were analysed and it was concluded that, although important, they were not enough to account for the measured size effect. Here, the dissipated energy at the very end of the test is analysed. It is shown that this energy cannot be neglected for small specimens if the tests are interrupted at a reasonably low rotation. When this energy is taken into account, the final values of G_F appear to be almost size-independent. This result supports G_F as a material parameter and provides further confidence in the RILEM proposal. Moreover, it furnishes a physical explanation for the perturbed ligament model previously developed by the authors.

1. INTRODUCTION

The specific fracture energy G_F has proved to be a useful parameter for design with concrete and cementitious materials [1] and for modelling the fracture behaviour of cohesive materials [2,3]. Nevertheless, available measures of G_F obtained with the work of fracture method applied to notched beams [4] provide values that change with sample size and, in general, show a trend towards an increase with specimen size [5–7].

As already pointed out in a previous paper [8], this apparent size-dependence of G_F calls into question the possibility of considering G_F as a material parameter. The only way to remove this doubt is to find some shortcomings in the determination of G_F that would explain this size effect as an artefact rather than an intrinsic feature of the material.

A systematic search for possible sources of experimental errors was undertaken by the authors. In two previous papers [8,9] the role of the testing equipment, the experimental set-up and the energy dissipation in the specimen bulk were analysed. In all cases, some energy dissipation increasing with specimen size was found. For beam depths ranging from 5 to 30 aggregate sizes, the maximum relative increment for G_F due to the testing equipment was less than 0.6%. The bulk energy dissipation, generated at regions of high tensile stresses, contributes at most 2%. The major contribution comes from the energy dissipation at the supports due to crushing and friction. This energy dissipation can account, at most, for a 15% increase. Anyhow, putting all these values together gives a size-dependence which is not enough to account for the observed size dependence, about 50% in our experiments.

The final key to solve this problem seems to be that – in bending – the test cannot be controlled up to absolute breakage of the specimen. Rather, the test must be stopped somewhere before that point and some energy, that corresponding to the unrecorded tail of the P–δ curve, is not accounted for in the measurements. A careful analysis of this neglected energy shows that it may account for the remaining 32% needed to obtain a real size-independent G_F value. This analysis is the subject of the first part of this paper. As an interesting consequence of this analysis, it is found that the P–δ tail correction is consistent with the perturbed ligament model (PLM) previously developed by the authors on phenomenological grounds [10–12]. The PLM provides, then, a practical procedure to extract a 'true' G_F value from a set of apparently size-dependent G_F measurements.

In the second part of this paper all the adjustments for G_F – those previously analysed [8,9] and that used in this paper – are applied to a set of G_F values obtained in testing concrete beams of four sizes. The results show that when the energy corresponding to the tail of the P–δ curve is taken into account, an almost size-independent G_F value is obtained.

2. THE P–δ TAIL IN A BENDING BEAM TEST

To estimate the energy dissipated at very low loads – when the load tends to zero in the descending branch of the P–δ diagram – one needs to model the beam behaviour when the cohesive crack closely approaches the free surface.

For cohesive materials and beams where *weight is compensated*, the last phase of a stable three-point bend test can be modelled following the rigid-body kinematics used by Petersson [13]. In this approach one assumes that the beam is divided into two rectangular

0025-5432/92

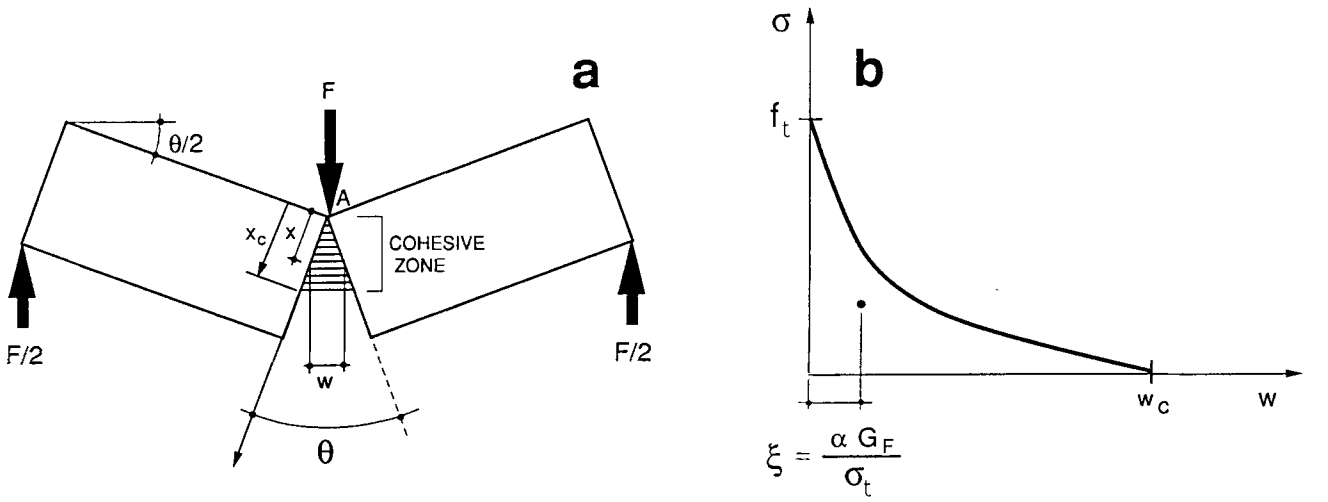

Fig. 1 (a) Rigid-body kinematics for the final stages of the bending test. (b) Softening function and abscissa of the centroid.

pieces which are connected only through the fracture zone, as sketched in Fig. 1. Also, it is assumed that the sides of the crack and the fracture zone are plane and that the compression zone is concentrated on a point at the top of the beam. Clearly this is an approximation because there always exists a compression zone at the top of the beam, which has however been proved to be asymptotically exact in the case of rectangular softening (Dugdale model with stress cut-off) [14].

The crack opening w at a certain distance x from A, as shown in Fig. 1a, will be given by

$$w = 2x \sin(\theta/2) \approx \theta x \tag{1}$$

Assuming a known softening function, the central bending moment may be written as

$$M = \int_0^{x_c} \sigma(w) B x \, dx = B \int_0^{x_c} \sigma(\theta x) x \, dx$$
$$= \frac{B}{\theta^2} \int_0^{w_c} \sigma(w) w \, dw \tag{2}$$

where M is the bending moment, $\sigma(w)$ is the softening function (as sketched in Fig. 1b), B is the beam thickness and x_c the point at which the softening is complete, hence $w(x_c) = w_c$. This result may be written as

$$M = \frac{\alpha B G_F^2}{f_t \theta^2} \tag{3}$$

because the integral in Equation 2 is the first-order moment of $\sigma(w)$ and can be expressed as the area enclosed between the positive axes and the softening curve, G_F, times the abscissa, ξ, of the centroid of that area. This distance can always be written as $\alpha G_F/f_t$, where f_t is the tensile strength (as shown in Fig. 1) and α a suitable parameter depending on the shape of the softening functions; for a rectangular softening $\alpha = 1/2$, for linear softening $\alpha = 2/3$ and for exponential softening $\alpha = 1$.

Equation 3 may be rewritten as

$$\frac{M}{B} = A\theta^{-2} \qquad A = \frac{\alpha G_F^2}{f_t} \tag{4}$$

which indicates that in a plot of M/B versus θ^{-2} the trend for large θ values is that of a straight line of size-independent slope A. The asymptotic P–δ curve is obtained from the equations above by setting

$$M = \frac{PS}{4} \qquad \theta = \frac{4\delta}{S} \tag{5}$$

so that

$$P = BSA \frac{1}{4\delta^2} \tag{6}$$

In a *weight-compensated* testing set-up, the zero load is not known with great precision because the *exact* weight distribution is not known. If the beam were completely broken at test stop, this final reading would be, by construction, the 'zero load' [10]. However, the beam approaches this level asymptotically, as shown in Fig. 2, and the load at test stop, P_f, is slightly larger than zero (this has been somewhat exaggerated in Fig. 2). Unfortunately the true zero is not known, as already pointed out, and the test stop point B must be taken as

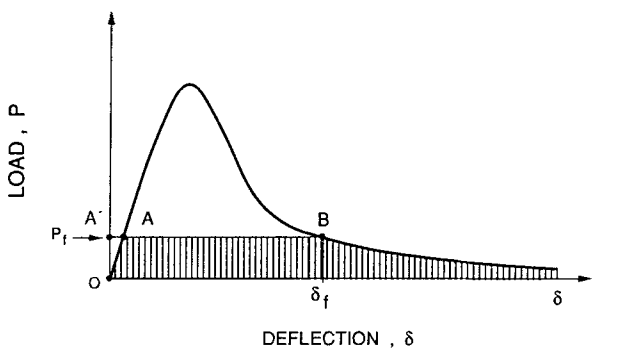

Fig. 2 Neglected energy when the test is interrupted at point B (point B is taken to correspond to zero load).

Table 1 Concrete properties

Proportional mixing, by weight				Concrete strength (MPa)		
Cement	Coarse	Fine	Water	Compressive	Tensile	Modulus
1	1.35	3.02	0.55	33.1	2.8	26 600

Cement content 400 kg m^{-3}; strength results at 28 days.

the 'practical zero'. The area that one can determine with bounded error is the area enclosed by the curve over the segment AB, which is taken as the best approximation of the total work of fracture W. The uncounted work of fracture is then the dashed area in Fig. 2, which we denote as ΔW_{Tail}. (A more rigorous treatment of this approximation based on the use of the complementary work instead of the ordinary work may be found elsewhere [10].)

To estimate ΔW_{Tail} we neglect the small triangular area OAA', and letting δ_f be the deflection at the point of test stop, B, the shaded area may be written, with the help of the approximate P–δ relation (Equation 6),

$$\Delta W_{Tail} = P_f \delta_f + \int_{\delta_f}^{\infty} P \, d(\delta) = \frac{BSA}{4\delta_f} + \frac{BSA}{4\delta_f} = \frac{BSA}{2\delta_f} \quad (7)$$

and the total measured fracture work W will be

$$W = G_F Bb - \Delta W_{Tail} = G_F Bb - \frac{BSA}{2\delta_f} \quad (8)$$

where b is the initial beam ligament ($b = D - a$). This can be rewritten as

$$W = G_F B\left(b - \frac{SA}{2G_F\delta_f}\right) = G_F B(b - b_0) \quad (9)$$

where

$$b_0 = \frac{SA}{2G_F\delta_f} \quad (10)$$

According to the RILEM procedure [2] the measured fracture energy would be evaluated as

$$G_{FMeas} = \frac{W}{Bb} = G_F\left(1 - \frac{b_0}{b}\right) \quad (11)$$

while the true fracture energy is, from Equation 9,

$$G_F = \frac{W}{B(b - b_0)} \quad (12)$$

When the rotation angle at which the test is stopped is the same for all the specimen sizes (which is the case for our tests and may be very usual) the fraction S/δ_f is constant and so is b_0. In such case Equation 12 coincides with that derived by the authors on phenomenological grounds in what was called the perturbed ligament model (PLM) [10–12]. The above equation may be read, then, as saying that a premature interruption of the tests at some fixed rotation angle produces the same effect as having a portion of ligament of length b_0 not contributing to the overall dissipation. b_0 coincides, then, with what was called the perturbed length. The above results provide an alternative physical support for the PLM equation.

3. EXPERIMENTAL PROCEDURE

Concrete notched beams were tested following, essentially, the RILEM recommendation for the measurement of G_F [2]. Details of materials and experimental procedures have already been published [12] and therefore only the relevant aspects will be briefly summarized here.

The concrete was a standard RILEM concrete, as described by Dutron [15]. Natural rounded aggregates, classified as siliceous, were used. Table 1 summarizes the characteristics of the concrete mix and some concrete properties measured according to ASTM standards. The aggregate maximum size was 10 mm.

Test specimens were notched beams, as sketched in Fig. 3; their dimensions are listed in Table 2. All specimens were cast in steel moulds and compacted with a vibrating

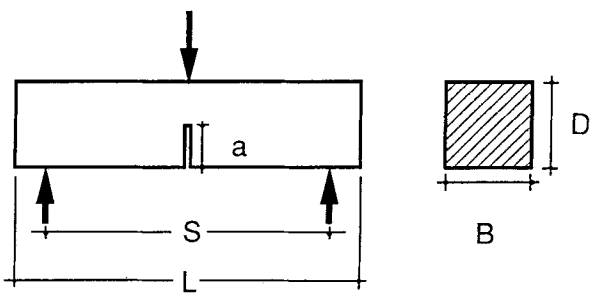

Fig. 3 Specimen dimensions.

Table 2 Test specimen dimensions (see Fig. 3)

Specimen	D (mm)	S (mm)	a (mm)	L (mm)	B (mm)
FT1	50	125	17	300	100
FT2	100	250	33	550	100
FT3	200	500	67	550	100
FT4	300	750	100	800	100

table. After demoulding, samples were stored under lime-saturated water until testing time.

Testing was performed in a 1 MN servohydraulic testing machine (Instron 1275), run in CMOD control mode. Loads were measured with a 25/50 kN load cell with a resolution of 1.25/2.5 N and 0.5% accuracy. CMOD was measured by a clip-on gauge MTS 632.03C-51, with 0.2 μm resolution and ±2 μm accuracy.

Deflection was measured as the relative displacement of the central loading head and the line defined by the points on the upper surface of the specimen located on the verticals of the lower supports. The displacement was measured by an extensometer located in a transverse hole in the loading head. The accuracy of the extensometer was better than 5 μm.

In all tests *weight compensation* was used. This was automatically accomplished by using specimens twice as long as the loading span for the two smallest sizes. Prestressed springs on both sides of the notch provided the load compensation for the larger specimens.

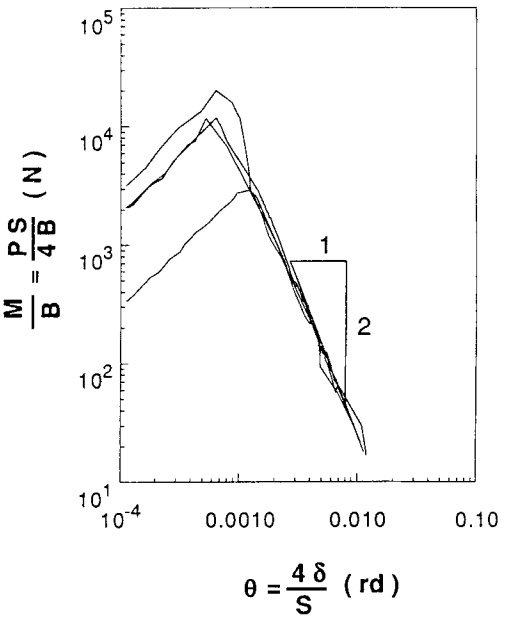

Fig. 4 Log–log plot of the experimental M–θ curve showing the $M \propto \theta^{-2}$ dependence at large rotations for all sizes.

4. RESULTS

4.1 Experimental values

Tests were performed on geometrically similar notched beams of the same thickness but of different sizes, as shown in Fig. 3. Experimental values are summarized in Table 3. All the results are mean of two specimens. Values in square brackets indicate half-range.

The energy of fracture G_F for each size was obtained according to the RILEM procedure [2] by dividing the measured work of fracture W by the ligament area:

$$G_{FMeas} = \frac{W}{Bb} \tag{13}$$

where the ligament b as already stated, is $b = D - a$, according to Fig. 3.

These G_{FMeas} results show a definite effect of the specimen size on the values of the fracture energy. When all possible sources of energy dissipation discussed in previous papers [8,9] and the effect of interrupting the test at some fixed rotation angle considered here are taken into account, an almost size-independent G_F emerges, as will be shown later on.

Table 3 Concrete fracture energy G_F (RILEM)

Sample	D (mm)	P_U (kN)	f_N (MPa)	G_{FMeas} (N m^{-1})
FT1	50	2.89[0.05]	4.31	57 [2]
FT2	100	5.21[0.06]	4.15	75[13]
FT3	200	9.37[0.06]	3.92	82 [2]
FT4	300	11.25[0.58]	3.08	94 [5]

P_U is the maximum load and $f_N = 1.5P_US/B(D-a)^2$ (see Fig. 3).

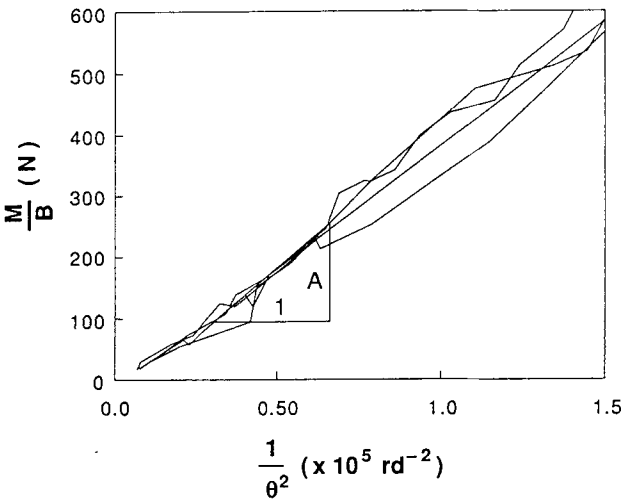

Fig. 5 M–θ^2 plot of the experimental M–θ curve showing the $M \propto \theta^{-2}$ dependence at large rotations for all the sizes.

4.2 Validation of the asymptotic equation for the P–δ curve tail

To check the accuracy of the model discussed in section 2 – or more specifically, Equations (4) – the P–δ curve is transformed into an M–θ curve using Equations 5. This M–θ curve is plotted in a log–log plot in Fig. 4. As can be seen, for large θ all the plots merge into a straight line of slope −2, as expected, because Equation 4 may be written as

$$\log \frac{M}{B} = \log A - 2 \log \theta \tag{14}$$

The value of A can be computed by extrapolation in Fig. 4 or, simply by adjusting a straight line to the M versus θ^{-2} plots for large values of θ, as shown in Fig. 5.

Table 4 Corrections for G_F in N m^{-1}

Source	Size 1	Size 2	Size 3	Size 4
G_{FMeas}	57 [2]	75 [13]	82 [2]	94 [5]
$-\Delta G_F$ (hysteresis)	−0.0	−0.2	−0.2	−0.5
$-\Delta G_F$ (bulk)	−0.5 (0.2)	−1.0 (0.3)	−1.5 (0.4)	−1.7 (0.5)
$-\Delta G_F$ (lateral supports)	−3.4 (1.0)	−1.8 (0.5)	−1.8 (0.7)	−2.0 (0.2)
$-\Delta G_F$ (central support)	−3.9 (1.5)	−4.8 (1.5)	−6.8 (1.6)	−7.2 (1.4)
G_{F1}	49.1	67.2	71.7	82.6
ΔG_{FTail}	22 (8)	18 (8)	7 (2)	6 (4)
G_F (corrected)	71 {13}	85 {23}	79 {7}	89 {11}

Values in square brackets indicate half-range. Values in parentheses indicate standard deviations. Values in braces { } are estimated variation intervals.

All these results support the suitability of the model for our purposes. From the knowledge of A, G_F and f_t, it is possible to estimate the value of α from Equations 4. For this concrete, where $G_F = 81$ N m^{-1} and $f_t = 2.8$ MPa, one obtains $\alpha = 2.1$.

This value of α is rather larger than those that can be directly derived from the usual analytical expressions for the softening curve, such as the bilinear curve proposed by Petersson [13], the pure exponential curve or the modified exponential of Reinhardt *et al.* [16] which deliver values of α ranging from 1 to 1.3. The fundamental reason for this discrepancy seems to be that the analytical proposals fit very well the experimental results for small and medium crack openings while the fit for large openings is rather poor, the experimental results displaying a much longer tail than the analytical fits. This causes little or no effect on the predicted results for small deflections of the beams (for usual laboratory sizes), because then only the initial portion of the softening curve comes into play. The divergence arises, however, when analysing a large deflection range as we do here.

That the discrepancy between analytical fits and experimental results may be large in the softening far end is obvious from the fits displayed in the above references [13,16] but it is clearer in the results of Rokugo *et al.* [17] which display a critical crack opening about three times larger than the Petersson fit. From Fig. 5 of the work of Rokugo *et al.* an estimate of the position of the centroid of the area enclosed by the experimental softening curve may be given. The centroid turns out to be around $w \approx 0.084$ mm, which in dimensionless terms corresponds to $\alpha \approx 1.9$, a value much closer to our result than to those of the analytical fits. This gives further support to our theoretical analysis, although further work is necessary to enhance the experimental support.

Once A is known, the 'perturbed ligament length', b_0, defined in Equation 10, can be evaluated from the value of the rotation angle $4\delta_f/S$ at which the tail of the experimental curve was cut. Using the average value from the test records, $4\delta_f/S = 0.012$, an estimated perturbed length $b_0 \approx 12$ mm is obtained, in agreement with the result delivered by the empirical procedure used previously [12]. This consistency provides further support for the present analysis and for the PLM equation.

5. ADJUSTMENT FOR G_F (RILEM)

The results of the two previous papers [8,9] indicated that several sources of spurious energy dissipation exist which are not usually taken into account when computing the specific fracture energy G_F. In the present work, it has been found that a non-negligible amount of energy may be neglected when cutting the tail of the P–δ curve. The next step is to analyse whether there is a significant improvement when all these corrections for the measured G_F are taken into account. The best estimate of G_F can then be written as

$$G_F = G_{FMeas} - \sum \Delta G_F + \Delta G_{FTail} \qquad (15)$$

where the sum is extended to all extra dissipation sources.

In Part 1 of this work [8] it was concluded that some energy dissipation due to hysteresis of the testing machine may occur and that this was specimen size-dependent. The energy dissipated for each beam size may be evaluated from Fig. 6 (Fig. 2a from [8]) with the knowledge of the average maximum load for each beam size reported in Table 3. The values of dissipated energy appear in Table 4.

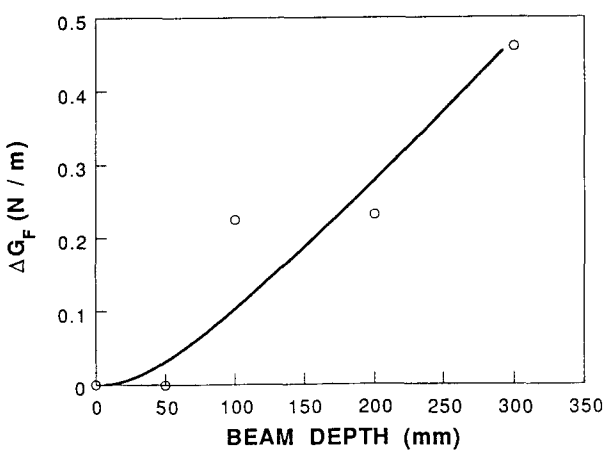

Fig. 6 Correction due to hysteresis in the measuring system (measured in [8]).

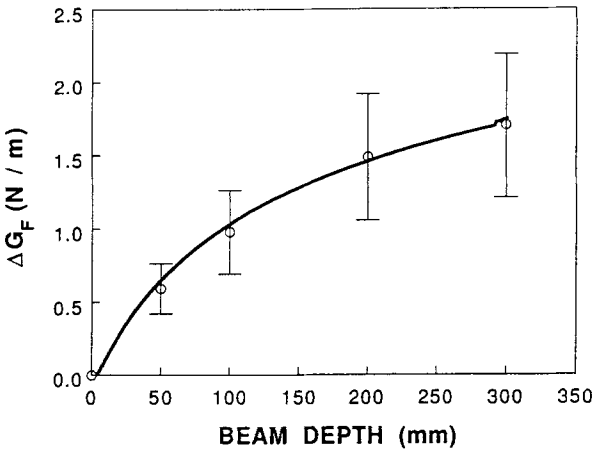

Fig. 7 Correction due to bulk dissipation (computed in [9]).

In Part 2 [9] it was shown that, apart from the surface energy, some energy was dissipated in the bulk of the material as the crack propagates. This bulk energy is dissipated at regions of high tensile stresses and the result, as a function of the beam depth, is shown in Fig. 7 (Fig. 8a from [9]). This dissipated energy is also reported in Table 4.

Supports are the major source of energy dissipation. Dissipation in the rolling supports, due to friction and to crushing, was discussed and measured in Part 1 [8]. For our tests, only friction must be accounted for, because the displacement measurement already excluded the crushing component. Dissipation at the central support, due to crushing, was considered and measured in Part 2 [9]. The result of both sources of spurious energy waste is represented in Fig. 8. Again, from the knowledge of the maximum loads for the different beam sizes, the values of dissipated energy at the supports were computed. To emphasize the different contributions from the lateral and central supports, both results appear in Table 4.

When all these sources of energy dissipation – not essential for fracturing – are taken into account and deducted from the measured energy, an intermediate estimate of G_F, G_{F1}, is obtained. Such results also appear in Table 4 and, unfortunately, still exhibit a non-negligible size effect (about 60% for the sizes considered).

As is shown in this paper, there is some amount of energy consumed in breaking the beam that has not been accounted for when testing is prematurely stopped. This energy is, from Equation 7,

$$\Delta W_{\text{Tail}} = \frac{BSA}{2\delta_f} \tag{16}$$

and depends only on the rotation angle $4\delta_f/S$ at which the tail of the P–δ curve is cut, apart obviously from fixed material parameters. When all tests are stopped at the same rotation angle, this energy will be size-independent, and when divided by the specimen ligament the specific fracture energy correction will decrease with specimen size.

The value of ΔT_{Tail} for each concrete beam size was obtained in the following way. Thickness B, loading span S and the deflection at which tests were cut, δ_f, were computed as the average values for the specimens of that size. A was obtained as the average slope of the M–θ^{-2} curves for all the sizes shown in Fig. 5. Finally, the values of the correction terms ΔG_{FTail} were computed as

$$\Delta G_{\text{FTail}} = \frac{\Delta W_{\text{Tail}}}{bB} \tag{17}$$

The values of this correction are shown, for each size, in Table 4, together with the final corrected values of G_F, which appear to have a much milder size dependence, if any at all. To illustrate this, such results are plotted in Fig. 9 as a function of specimen size. As can be easily realized, they are almost size-independent. The average value is 81 N m^{-1}, and no definite trend may be guessed in view of the large scatter band which comes from the addition of the scatter of all the measurements and corrections.

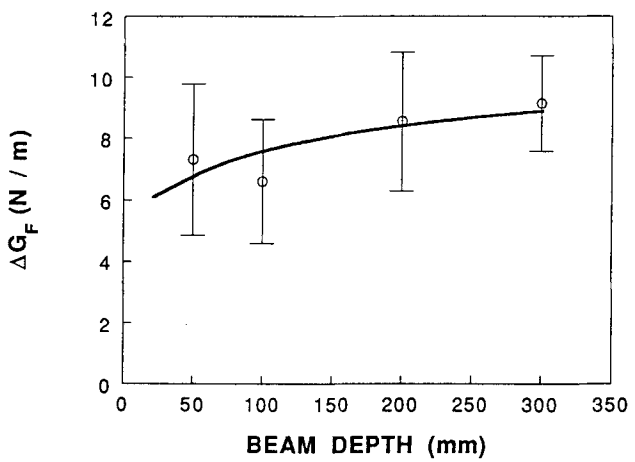

Fig. 8 Correction due to dissipation at the supports (measured in [8] and [9]).

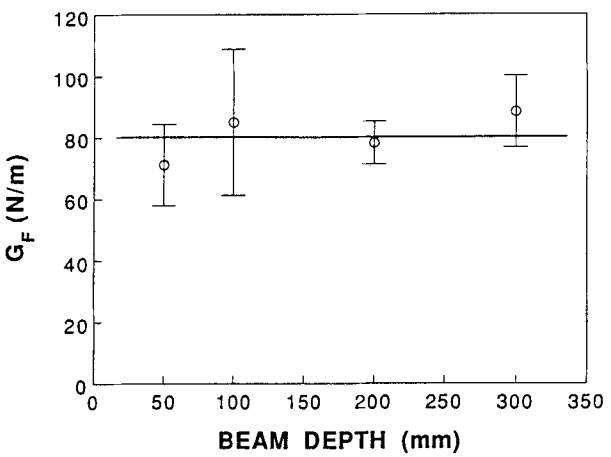

Fig. 9 Final corrected values of the fracture energy versus size of the specimen: the size effect on G_F has essentially disappeared.

6. CONCLUSIONS

The purpose of this paper, and two previous ones [8,9], was to ascertain possible sources of energy dissipation in addition to that essential for the fracture process which are not taken into account when determining G_F following the RILEM recommendation based on the work of fracture. Several sources were detected and the corresponding dissipated energy was computed or measured. Unfortunately, after taking into account all these energy corrections, the final value of the specific fracture energy still exhibits a marked dependence on specimen size.

1. In this paper, attention was focused on the dissipated energy, often neglected, in weight compensated tests at the very end of the test. In practice, tests are stopped at a certain value of the displacement, or bending angle, and the remaining dissipated energy neglected. Here it was shown that this energy cannot be neglected for small specimens if the tests are interrupted at a reasonably low rotation.

2. When this energy is taken into account, the final values of G_F appear to be almost size-independent for the experimental results of the authors. This result supports considering G_F as a material parameter for design purposes and provides further confidence in modelling concrete and rocks as cohesive materials.

3. The energy enclosed in the P–δ tail justifies and provides a physical explanation for the perturbed ligament model, previously developed by the authors on phenomenological grounds. The work of fracture obtained when this energy is neglected turns out to be equal to the work of fracture one would obtain if a portion of the ligament – the perturbed length – were destroyed (or perturbed) prior to the start of the test.

ACKNOWLEDGEMENTS

The authors gratefully acknowledge financial support for this research provided by the Comisión Interministerial de Ciencia y Tecnología CICYT, Spain, under grant PB86-0494, and by the Polytechnical University of Madrid under grant A-91 0020 02-31.

REFERENCES

1. Hillerborg, A., 'The theoretical basis of a method to determine the fracture energy G_F of concrete', *Mater. Struct.* **18**(106) (1985) 291–296.
2. RILEM TC-50 FMC (Draft Recommendation), 'Determination of the fracture energy of mortar and concrete by means of three-point bend tests on notched beams', *ibid.* **18**(106) (1985) 285–290.
3. Elices, M. and Planas, J., 'Material models', in 'Fracture Mechanics of Concrete Structures' (Chapman & Hall, London, 1989) pp. 16–66.
4. *Idem.*, 'Size effect and experimental validation of available fracture models', in 'Analysis of Concrete Structures by Fracture Mechanics' (Chapman & Hall, London, 1990 pp. 99–127).
5. Hillerborg, A., 'Results of three comparative test series for determining the fracture energy G_F of concrete', *Mater. Struct.* **18**(107) (1985) 407–413.
6. Wittmann, F. H. (Ed.), 'Fracture Toughness and Fracture Energy of Concrete' (Elsevier, Amsterdam, 1986).
7. Mihashi, H., Takahashi, H. and Wittman, F. H. (Eds.), 'Fracture Toughness and Fracture Energy: Test Methods for Concrete and Rock' (Balkema, Rotterdam, 1989).
8. Guinea, G. V., Planas, J. and Elices, M., 'Measurement of the fracture energy using three-point bend tests: 1 – Influence of experimental procedures', *Mater. Struct.* **25**(148) (1992) 212–218.
9. Planas, J., Elices, M. and Guinea, G. V., 'Measurement of the fracture energy using three-point bend tests: 2 – Influence of bulk energy dissipation', *ibid.* **25**(149) (1992) 305–312.
10. Planas, J. and Elices, M., 'Conceptual and experimental problems in the determination of the fracture energy of concrete', in 'Fracture Toughness and Fracture Energy: Test Methods for Concrete and Rock' (Balkema, Rotterdam, 1989) pp. 165–181.
11. Planas, J., Maturana, P., Guinea, G. V. and Elices, M., 'Fracture energy of water saturated and partially dry concrete at room and at cryogenic temperatures', in 'Advances in Fracture Research' (Pergamon, Oxford, 1989) pp. 1809–1817.
12. Maturana, P., Planas, J. and Elices, M., 'Evolution of fracture behaviour of saturated concrete in the low temperature range', *Engng Fract. Mech.* **35** (1990) 827–834.
13. Petersson, P. E., 'Crack Growth and Development of Fracture Zones in Plain Concrete and Similar Materials', Lund Institute of Technology Report TVBM-1006 (1981).
14. Planas, J. and Elices, M., 'The influence of specimen size and material characteristic size on the applicability of effective crack models', in 'Fracture Processes in Concrete, Rock and Ceramics' (Chapman & Hall, London, 1991 pp. 375–385).
15. Dutron, P., 'Mise au point d'une composition de béton de référence pour recherches et essais en laboratoire', *Mater. Struct.* **7**(39) (1974) 207–224.
16. Reinhardt, H. W., Cornelissen, H. A. W., and Hordijk, D. A., 'Tensile tests and failure analysis of concrete', *J. Struct. Engng ASCE* **112**(11) (1986) 2462–2477.
17. Rokugo, K., Iwasa, M., Suzuki, T., and Koyanagi, W., 'Testing methods to determine tensile strain softening curve and fracture energy of concrete', in 'Fracture Toughness and Fracture Energy' (Balkema, Rotterdam, 1989) pp. 153–163.

RESUME

Mesure de l'énergie de rupture par les essais de flexion trois points: 3 – Qu'en est-il si on retranche le segment *P–δ*?

Les mesures de l'énergie de rupture G_F *obtenues selon la méthode préconisée par la Commission Technique 50, dont on dispose, fournissent des valeurs qui se trouvent changer avec la taille de l'éprouvette, ce qui met en question la possibilité de considérer* G_F *comme un paramètre du matériau. Dans les articles précédents, on a examiné plusieurs sources de dissipation de l'énergie, et on a conclu que, tout en ayant de l'importance, elles ne suffisent pas à expliquer l'effet d'échelle mesuré.*

Une solution semble résider dans le fait que, en flexion, l'essai ne peut être contrôlé jusqu'à rupture complète de l'éprouvette. Il doit être stoppé quelque part avant ce point, et la quantité d'énergie qui correspond au segment non enregistré de la courbe P–δ *n'est pas prise en compte dans les mesures. Quand cette énergie est prise en compte, dans les résultats expérimentaux des auteurs, les valeurs, finales de* G_F *semblent presque indépendantes de l'échelle. Ce résultat permet de considérer* G_F *comme un paramètre du matériau à des fins de calcul, et constitue un encouragement pour la modélisation du béton en tant que matériau cohérent.*

L'énergie comprise dans le segment P–δ *justifie une explication physique du concept phénoménologique dit 'Perturbed Ligament Model' que les auteurs ont précédemment élaboré.*